Multiple Degrees of Freedom Active Motion Control of a Hydraulically Actuated Crane

Marius Balan*
Deptartment of Design Manufacturing Engineering Management, University of Strathclyde
Glasgow, United Kingdom
mariusliviu.balan@strath.ac.uk

Pawel Majecki
Industrial Systems and Control Ltd
Glasgow, United Kingdom
pawel@isc-ltd.com

Michael Grimble
Department of Electronic and Electrical Engineering, University of Strathclyde
Glasgow, United Kingdom
m.j.grimble@strath.ac.uk

Paul Blackwell
Deptartment of Design Manufacturing Engineering Management, University of Strathclyde
Glasgow, United Kingdom
paul.blackwell@strath.ac.uk

Abstract*— As offshore wind farms become larger and further from the shore, there are strong economic and climate incentives to perform transfers required for operations and maintenance from floating vessels, rather than employing expensive and slow jack up rigs. However, successful transfers of heavy and sensitive equipment from a floating vessel (in all but benign sea/wind conditions) are heavily dependent on multiple degrees of freedom (DoF), high performance control. Two control design methods were employed to assess the viability of heavy lifts from floating vessels through a simulation approach using Simulink. The crane system was first modelled to operate under simulated vessel motions given by sea states with a significant wave height of 5 m and maximum wave frequency of 1 rad/s. Then, traditional control (feedback and feedforward) was designed to achieve motion compensation with steady-state position errors under 20 cm. To achieve an improved performance, a more robust controller architecture was required, thus the nonlinear generalized minimum variance (NGMV) control algorithm was chosen for this application. Due to its ability to compensate for significant system nonlinearities and the ease of implementation NGMV was a good candidate for the task at hand. Tuning the controller parameters to stabilize the system can also be based on previous classical, say PID, control solutions. Simulations showed NGMV provided an improved control performance compared to traditional control when considering model mismatch.

Keywords*— system modelling, offshore wind Operation and Maintenance, nonlinear generalized minimum variance control, feedback and feedforward control

I. INTRODUCTION

Due to a wider available surface and steadier wind at sea, offshore wind turbines are built in ever larger size and thus are able to increase their capacity and produce more energy. Moving wind farms to offshore sites involves however a larger investment than onshore as Operation and Maintenance (O&M) of a wind turbine accounts for around 25% of its lifetime cost [1] and carbon emissions [2]. According to the Life Cycle Assessment studies presented in [2] [3], transfers by ship or helicopter contribute for 17% of emissions and the jack-up rigs, used for transferring heavy equipment, account for approximately 33% of CO2 emissions. Thus, optimising accessibility to the windfarm for O&M will also lower the greenhouse gas emissions.

Project supported by the EU INTERREG VA Programme, managed by the Special EU Programmes Body (SEUPB), with match funding provided by the Department for the Economy (Northern Ireland) and the Department of Enterprise, Trade and Employment (Republic of Ireland). Grant number IVA5033

Research [4] shows a proportional relation between accessibility to wind farm, turbine's availability and expenses minimization. The requirements for improved accessibility consist of: employing a floating vessel, multiple degrees of freedom (DoF) active motion control, operation in sea states with wave heights of 2.8 m. The solution should not require any special provisions on the turbine (such as landing pads for helicopter access).

This research investigates control methods to assess whether a crane on a moving vessel can be controlled to safely manipulate heavy components (in the range of tens of tons). This viability study is conducted by following a simulation approach in Simulink.

Feedback and feedforward controls are used in conjunction to allow compensation for measured and unmeasured disturbances [5]. Feedforward is commonly used in the servo valve control of hydraulic pistons in robotic arms. Given a desired trajectory reference, cylinder velocity, acceleration and jerk can be derived and multiplied by feedforward gain then summed with the PID terms. For example, Küchler and Sawodny [6] studied a two-stage feedforward control algorithm for active heave compensation. First, a feedforward controller decoupled payload motion from vessel crane tip. Then, a 2 DoF feedforward controller and a state feedback were used for trajectory tracking and disturbances stabilisation. Future work should include an observer-based estimation to compensate for undesired payload displacement offset caused by parameter uncertainties.

The NGMV control was developed for nonlinear multivariable processes in both state-space and polynomial versions [7]. This scheme is employed to compensate for the nonlinearities in all relevant parts of the model. NGMV control applied for state dependent multivariable models [8] involves the plant nonlinearities directly and does not rely on linearization techniques as opposed to some other nonlinear controllers. This controller structure includes a delay free exact model of the plant, and error and the control weightings that remove any mismatch with the actual plant.

This paper will present a comparison between two control methodologies while aiming to achieve 3D active motion compensation for a crane system. Section II presents the system formulation including wave modelling, hydraulics, and system

dynamics. Section III details the design of the two control algorithms. In section IV, the simulation results show the performance comparison between a traditional controller and NGMV control.

II. System Modelling

A. System Description

Consider a 90 m tall hydraulic crane robot holding a 40 ton payload that is placed on a moving base with 3 degrees of freedom (DoF), i.e. translations along the x, y and z axes (as shown in Fig. 1). The goal is to move the payload over a predefined 3D trajectory while being decoupled from the effect of the base motions. To achieve that, 4 actuators (3 hydraulic cylinders and 1 motion actuator for the robot base) rotate the crane joints. The desired payload trajectory is converted into corresponding joint rotations via Inverse Kinematics (IK). The measured payload position is taken by placing a motion sensor at the crane end-effector (EE) relative to a fixed world reference frame (coinciding with the initial base position).

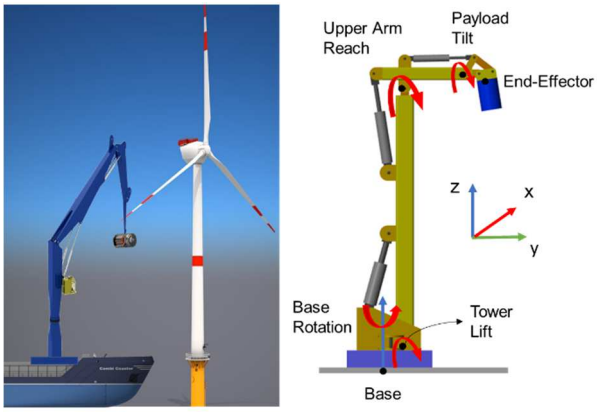

Fig. 1. Real-life scenario is presented on the left and a simplified Simulink representation of the hydraulic crane is displayed on the right

With respect to the diagram on the right in Fig. 1, payload translations are achieved by rotation of the four joints: 'Base Rotation' provides payload translation on x-axis, 'Tower Lift' moves the payload on the y-axis, 'Arm Reach' covers the up/down motion on the z-axis, while the last joint 'Payload Tilt' rotate the payload around the x-axis.

B. Wave modelling

Wave modelling and corresponding vessel motion are essential elements when designing active motion compensation systems that counteract wave induced ship motions. The main stages involved in simulating vessel motion on 6 axes (translations and rotations on x-y-z) are shown in Fig. 2.

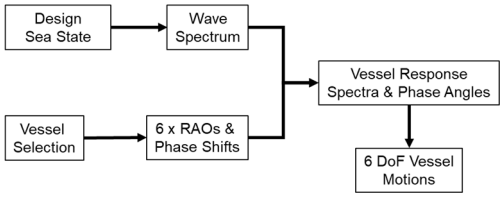

Fig. 2. Diagram describing the procedure to simulate vessel motions in 6 DoF

The sea state selected for the purpose of this work features a 5 m significant wave height and is a superposition of independent random harmonics with maximum wave frequency of 1 rad/s. A JONSWAP spectrum [9] was employed to obtain the wave components in terms of frequency and directionality. A vessel of length 175 m was chosen for this application to accommodate the hydraulic crane.

Having selected the sea state and the vessel dimension, the Marine System Simulator (MSS) toolbox [9] in Simulink was used to generate wave-induced ship motion profiles for translation axes on x-y-z. For example, heave motion time series can be written as in eq. (1):

$$r_z(t) = \sum_{m=1}^{M} \sum_{n=1}^{N} \{ RAO_z(\omega_n,\mu_m) * \zeta_{a,n,m} \cos[\omega_n t + \varepsilon_{n,m} + \varepsilon_{z\zeta}(\omega_n,\mu_m)] \} \quad (1)$$

with:

r_z	Heave [m]
m	Wave direction index number [-]
M	Number of wave directions [-]
n	Harmonic wave index number [-]
N	Number of wave frequencies [-]
RAO_z	Heave Response Amplitude Operator [-], defined as the ratio between vessel and wave amplitudes
ω_n	Angular frequency of wave n [rad/s]
μ_m	Wave direction m [rad]
$\zeta_{a,n,m}$	Amplitude of wave n travelling in direction m [m]
ε_n	Phase shift of wave n travelling in direction n [rad]
$\varepsilon_{z\zeta}$	Wave elevation to heave phase difference [rad]

C. Hydraulic actuator design

A double acting hydraulic actuator was employed to control each of the three joints presented in Fig. 1. The schematic diagram presented in Fig. 3 consists of a constant pressure supply pump, a servo valve, and the hydraulic cylinder.

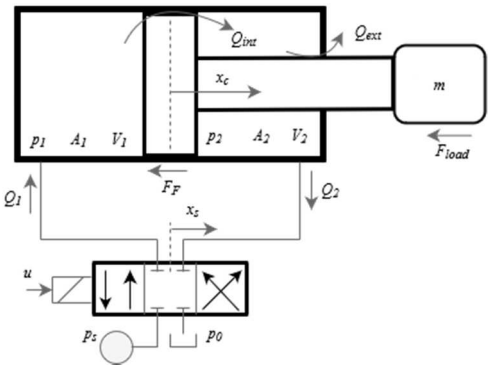

Fig. 3. Diagram of a hydraulic actuator

An example of modelling a nonlinear hydraulic actuator is presented in [10] along with the derivation of its state-space representation, which is given below in eq. (2):

$$\begin{aligned}
\dot{x}_1 &= x_2 \\
\dot{x}_2 &= \frac{1}{m}\left[x_3 A_1 - x_4 A_2 - F_F(x_2) - F_{load}\right] \\
\dot{x}_3 &= \frac{E_{oil}(x_3)}{V_{0,1}+A_1 x_1}\cdot\left[Q_1(x_3,x_5) - A_1 x_2 - Q_{int}(x_3,x_4)\right] \\
\dot{x}_4 &= \frac{E_{oil}(x_4)}{V_{0,2}+A_2 x_1}\cdot\left[Q_{int}(x_4,x_5) - Q_{ext}(x_4) - A_2 x_2 + Q_2(x_4,x_5)\right] \\
\dot{x}_5 &= x_6 \\
\dot{x}_6 &= \omega_n^2 u - 2B\omega_n x_6 - \omega_n^2 x_5
\end{aligned} \tag{2}$$

where:

x_1, x_c	Position of cylinder piston [m]
x_2, v_c	Velocity of cylinder piston [m/s]
x_3, p_1	Fluid pressure in chamber 1 [Pa]
x_4, p_2	Fluid pressure in chamber 2 [Pa]
x_5, x_s	Position of valve spool [m]
x_6, v_s	Velocity of valve spool [m/s]
A_1, A_2	Chambers 1 and 2 areas [m^2]
$Q_{1,2}$	Flow rate to chambers 1 and 2 [m^3/s]
Q_{int}, Q_{ext}	Internal and external leakage flows [m^3/s]
$V_{0,1/2}$	Initial fluid volume in chambers [m^3]
F_F, F_{load}	Friction and load forces [N]
β	Fluid bulk modulus [Pa]
m	Load mass [kg]
B, ω_n, u	Valve damping [-], natural frequency [rad/s] and input voltage [V]

Systems with high natural frequency ω_n are easier to control and as a rule of thumb it should be at least 4 times the desired frequency of acceleration. In this application, the pistons should have an acceleration frequency equal to the largest frequency component of the wave. ω_n can be increased by adjusting the parameters in eq.(3):

$$\omega_n = \sqrt{\frac{4\beta A^2}{Vm}} \tag{3}$$

The parameters in (3) can be modified to achieve the desired natural frequency. A fluid with a larger bulk modulus, larger cylinders (however slower valves), or a reduced load mass can be selected to increase ω_n.

D. Crane dynamics

Crane dynamics influence how each piston displacement influence its corresponding joint rotation. The dynamics are determined by the inertia of the load attached to each actuator. Their inertiae vary according to the gravitational force acting on the loads. For example, the lift actuator experiences more force when the tower is lowered compared to its initial upright position.

The System Identification Toolbox in Matlab was used to correlate the piston displacement data to joint rotational data obtained after simulating the crane model in Simulink. Their linearized transfer functions are:

$$\begin{aligned}
H_{Lift(pist2jnt)} &= \frac{-0.05034z^{-1}+0.1047z^{-2}-0.05436z^{-3}}{z-2.988z^{-1}+2.979z^{-2}-0.9907z^{-3}} \\
H_{Reach(pist2jnt)} &= \frac{0.8924z^{-1}-1.858z^{-2}+0.9661z^{-3}}{1-2.795z^{-1}+2.602z^{-2}-0.8071z^{-3}} \\
H_{Tilt(pist2jnt)} &= \frac{9.312z^{-1}-14.83z^{-2}+5.515z^{-3}}{1-2.357z^{-1}+2.005z^{-2}-0.6485z^{-3}}
\end{aligned} \tag{4}$$

For the base rotation, a time-delayed motion actuation signal directly controls the revolute joint according to transfer function $H_{base} = \frac{1}{1-z^{-1}}$.

III. Control Methodology

A high-level diagram describing the control implementation within the crane system is presented in Fig. 4.

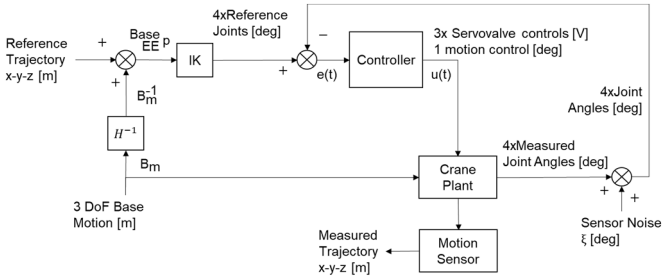

Fig. 4. High-level diagram consisting of the main components comprised in the control architecture of the crane system

The reference trajectory is given only in translations on x-y-z axes without considering any rotations. The measured trajectory is obtained by placing a motion sensor at the end-effector relative to the fixed world frame that coincides swith the initial location of the robot base.

The position vector ${}^{Base}_{EE}p$ describes the translation of the end-effector relative to the robot base as 3-element column vector $[x \quad y \quad z]$; this is obtained by summing the desired payload trajectory and the inverted robot base translations on x, y and z.

B_m and B_m^{-1} refer to the base and inverted base translation matrices that contain column vectors for translation and rotation motions obtained from the MSS toolbox given as: $B_m = [r_x \quad r_y \quad r_z]$ with r_x- surge, r_y – sway, and r_z – heave.

For the Inverse Kinematics (IK) algorithm, a robust numerical solution can be computed via Levenberg-Marquardt method in Simulink [11]. Even in cases where the problem does not have solutions or has countless solutions, the method converges to the optimum solution in the sense that it minimizes the residual from the target points with the smallest joint deviations.

A. Feedback and feedforward control

The feedback and feedforward control design is based upon the second order approximation of the hydraulic cylinder, which can be modelled as a mass between two springs. The transfer function between servo valve input voltage and piston displacement can be written as in eq. (5):

$$H_{cyl}(s)=\frac{x_c}{u}=\frac{K*\omega_n^2}{s*(s^2+2*\zeta\omega_n s+\omega_n^2)} \tag{5}$$

with damping ζ and natural frequency ω_n

1) PID with double derivative (PIDD) feedback control

Proportional gain K_P speeds up the response and reduces steady-state (ss) error, integral term K_I eliminates ss error but may lead to overshoot and derivative K_D term acts as a brake and stabilising factor with respect to integral term. A double derivative term K_{DD} is included to control system's natural frequency and damping, which would otherwise be dictated by mechanical/hydraulic design only.

The unfiltered controller transfer function of the PIDD is given in eq. (6):

$$C_{PIDD}(s)=K_P+\frac{1}{s}K_I+sK_D+s^2K_{DD} \tag{6}$$

The closed loop transfer function can be written as:

$$H(s)=\frac{H_{cyl}(s)C_{PIDD}(s)}{1+H_{cyl}(s)*C_{PIDD}(s)}= \\ =\frac{(sK_P+K_I+s^2K_D+s^3K_{DD})K\omega_n^2}{s^4+(2\zeta\omega_n+K\omega_n^2+K_{DD})s^3+(\omega_n^2+K_DK\omega_n^2)s^2+K\omega_n^2K_Ps+K\omega_n^2K_I} \tag{7}$$

The characteristic equation (7) will not overshoot, and the response will be that of a low-pass filter's in series. The poles are placed as far as possible to the left on the z-plane so that errors and transients decay to zero as fast as possible.

Due to the large sizing of the crane, it is desirable to design a slow response PIDD. Thus, the characteristic equation can be designed with two pairs of real poles (at $-\lambda$ and $-\mu$):

$$(s+\lambda)^4=s^4+4\lambda s^3+6\lambda^2s^2+4\lambda^3s+\lambda^4 \tag{8}$$

Equating the coefficients for each power of s between the actual characteristic equation in (7) and the desired characteristic equation (8) gave the PIDD gains:

$$K_I=\lambda^2\frac{\mu^2}{K\omega_n^2};\quad K_P=2\lambda\mu\frac{\mu+\lambda}{K\omega_n^2};\quad K_D=\frac{2\lambda\mu^2+2\lambda^2\mu-\omega_n^2}{K\omega_n^2}; \\ K_{DD}=2\frac{\mu+\lambda-\zeta\omega_n}{K\omega_n^2} \tag{9}$$

For stability, the following condition needs to apply: $\lambda+\mu\geq\zeta*\omega_n$. If λ is small, μ should be large enough so that K_d and K_{dd} are not negative. However, $e^{-\lambda t}$ will take longer to decay to zero so the response will be slower given changes in target positions and disturbances. If λ increases, then μ should decrease; the fastest response will occur when $\lambda=\mu=\frac{\zeta\omega_n}{2}$.

2) Feedforward control design

The ideal feedforward control gains can be extracted from the inverted transfer function of the hydraulic cylinder from eq. (5) as follows in eq. (10):

$$u_{FF}=H_{cyl}^{-1}(s)x_c=\frac{s(s^2+2\zeta\omega_n s+\omega_n^2)}{K\omega_n^2}x_c= \\ =\frac{1}{K}sx_c+\frac{2\zeta}{K\omega_n}s^2x_c+\frac{1}{Kw_n^2}s^3x_c \tag{10}$$

with feedforward velocity, $K_v=\frac{1}{K}x_c$; feedforward acceleration, $K_a=\frac{2*\zeta}{K*\omega_n}x_c$; feedforward jerk, $K_j=\frac{1}{K\omega_n^2}x_c$; feedforward steady-state slope gain, $K=\frac{v_c}{u}$

A real system cannot be precisely modelled. Implementing the ideal feedforward controller could result in reference tracking errors due to model mismatch. System mismatch was created by designing controllers for faster actuators, and then implementing the control law on a slower system. The actuators of the mismatched model had a lower natural frequency due to increasing their radius and increasing their valves' areas.

While PIDD parameters can be tuned to minimize the errors caused by model mismatch, the more robust NGMV controller was implemented to tackle this challenge.

B. NGMV control architecture

The architecture of the NGMV controller implemented in the crane system is presented as a diagram in Fig. 5.

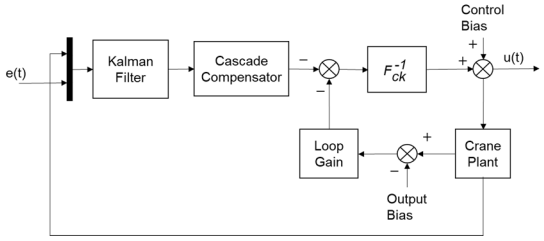

Fig. 5. NGMV control loop architecture

The main blocks found in Fig. 5 are described below:

1) Kalman filter

Kalman filter is required for state estimation, and it includes the plant, and the disturbance model states, as well as the states of the dynamic cost-function weightings. This is a time-varying estimator and is implemented as a recursive algorithm (as described in [12], Ch.15).

2) Crane plant

The model is defined as:

$$(Wu)(t)=z^{-k}W_{0k}(W_{1k}u)(t) \tag{11}$$

where W_{1k} is finite-gain stable nonlinear input subsystem and W_{0k} is the linear output subsystem. In this case, let W_{1k} describe the entire crane system and $W_{0k}=I_4$ (4x4 identity matrix to match the four-input four-output crane system).

3) Cascade compensator amd Loop Gain

The optimal control problem involves the minimization of the cost function:

$$J=E\{\phi_0^T(t)*\phi_0(t)\,|t\} \quad (12)$$

where:

$$\phi_0(t)=P_c(z^{-1})e(t)+(F_c u)(t) \quad (13)$$

with error signal $e(t)$, error weighting $P_c(z^{-1})=P_{cd}^{-1}(z^{-1})P_{cn}(z^{-1})$, control signal $u(t)$ and control weighting $(F_c u)(t)=z^{-\Lambda_0}(F_{ck}u)(t)$.

The cascade compensator and the loop gain are dictated by the selection of the reference model W_r, disturbance model W_d, linear subsystem W_{0k}, error weighting and control weighting.

The reference model was defined as a near integrator, which is the stochastic equivalent of step reference changes in the input payload trajectory:

$$W_r=\frac{1}{1-n_{int}*z^{-1}}*I_4 \quad (14)$$

where n_{int}=0.9999 and is the near-integrator term.

The disturbance model was written as a 2nd order system to match the wave motion profiles:

$$W_d=\frac{1}{\frac{1}{\omega_n}s^2+\frac{2\times\zeta}{\omega_n}s+1}*\frac{1}{n_{int}*s} \quad (15)$$

with natural frequency equal to wave frequency, ω_n=1 rad/s and an arbitrary selected damping ζ=0.5.

A near-integrator term was also added to account for unmeasured output disturbances.

4) Dynamic weightings, P_c and F_{ck}

The properties of the NGMV controller are often critically dependent on the selection of the dynamic cost-function weightings P_c and F_{ck} (Chapter 5 in [12]).

The error weighting was designed based on tuning the PID parameters determined in the previous experiments (Section A) for each actuator. Thus, a transfer function can be created:

$$C(z^{-1})=K_P+\frac{K_i}{1-n_{int}*z^{-1}}+K_d*(1-z^{-1}) \quad (16)$$

The formula for control weighting is given as:

$$F_{ck}(z^{-1})=-\frac{\rho(1-\gamma z^{-1})}{1-\gamma} \quad (17)$$

with:

ρ positive scalar; reducing ρ produces a faster response and a more aggressive control action

γ a lead term that influences controller's high frequency gain, $\gamma \in [0,1]$; $1/(1-\gamma)$ term decouples the lead term from the overall gain.

IV. Simulation Results

Simulations of the crane system were run in Simulink with each of the controllers used in the loop. In Fig. 6, the joint rotations tracking is displayed while Fig. 7 displays the error between the desired and measured outputs (joint angles).

The recorded payload trajectory was taken with respect to the fixed reference frame. The payload motion was displayed for each independent axis in Fig. 8 and as a 3D profile in Fig. 9.

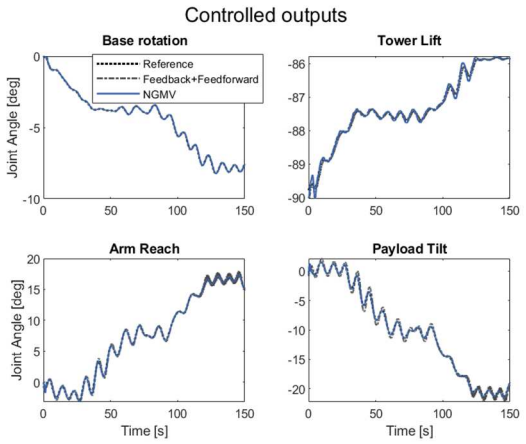

Fig. 6. Controllers' performance in terms of reference tracking of joint rotations using feedback and feedforward compared to NGMV

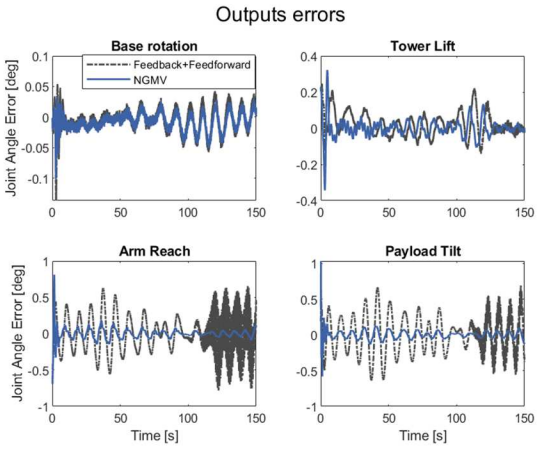

Fig. 7. Joint rotations errors showing the difference between the two controllers' performance

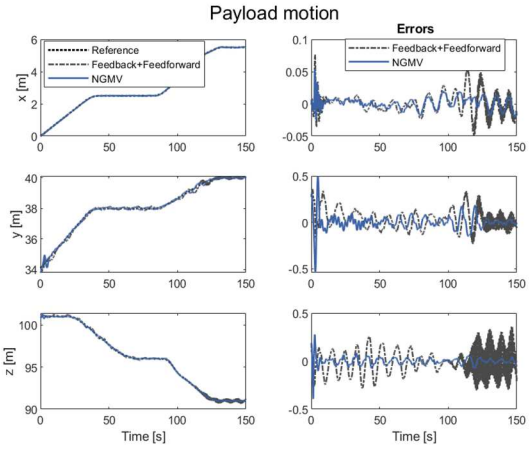

Fig. 8. Measured payload motion compared against the desired motion on each of the x, y, and z axes

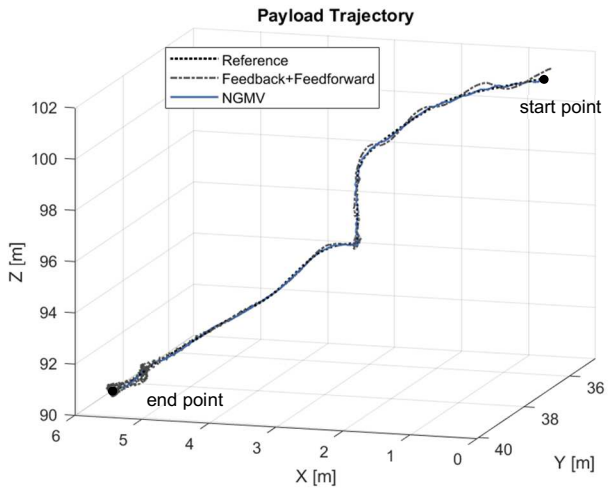

Fig. 9. Measured payload 3D trajectory with respect to the fixed reference frame

Simulations performed with PIDD and NGMV controllers in the loop produce comparable regulating performance in terms of reference tracking and disturbance rejection. This confirms the assertion that the PID-based NGMV weightings selection is a useful starting point for controller tuning.

V. Conclusions

This paper presented two control methods to achieve 3D active motion compensation for a hydraulic crane situated on a floating vessel. The work followed a simulation approach in Simulink. Given an arbitrary design of the crane, the wave-induced ship motions were determined via the MSS toolbox. Then, the hydraulics and dynamics of the crane were presented, followed by the design of two controllers. Initially, a traditional control, PIDD and feedforward, was implemented showing an acceptable performance of less than 20 cm error from setpoint at steady state. However, when accounting for model mismatch, a more robust control law was required. Thus, NGMV control was selected in that regard, also due to its ability to compensate for high system nonlinearities and ease of implementation based on tuning the previously determined PID parameters.

Results showed that traditional control performance degraded when away from the operating point. The NGMV controller offered an improved performance, being able to reduce motion oscillation while compared with the fixed gain PIDD control.

Future work will consider an in-depth investigation of controllers' robustness against model mismatch. Thus, various levels of uncertainty will be introduced to the hydraulic fluid bulk modulus and links masses (which influence actuators' natural frequency) to assess system sensitivity.

Prior to implementation of the real-sized system, scaled prototypes should be built and tested on land and on water to determine whether the control approach is viable. A thorough risk analysis will also be required to establish the insurances, certification and regulations before commercialization.

Acknowledgment

The authors would like to thank Dr. Dorothy Evans at Department of Design Manufacturing Engineering Management, University of Strathclyde, and Dr. Andy Clegg at Industrial Systems and Control Ltd, Glasgow for their valuable suggestions and support of the work.

References

[1] C. Röckmann, S. Lagerveld, and J. Stavenuiter, "Operation and Maintenance Costs of Offshore Wind Farms and Potential Multi-use Platforms in the Dutch North Sea," in *Aquaculture Perspective of Multi-Use Sites in the Open Ocean: The Untapped Potential for Marine Resources in the Anthropocene*, B. H. Buck and R. Langan, Eds. Cham: Springer International Publishing, 2017, pp. 97–113. doi: 10.1007/978-3-319-51159-7_4.

[2] B. Reimers, B. Özdirik, and M. Kaltschmitt, "Greenhouse gas emissions from electricity generated by offshore wind farms," *Renewable Energy*, vol. 72, pp. 428–438, Dec. 2014, doi: 10.1016/j.renene.2014.07.023.

[3] H. L. Raadal, B. I. Vold, A. Myhr, and T. A. Nygaard, "GHG emissions and energy performance of offshore wind power," *Renewable Energy*, vol. 66, pp. 314–324, Jun. 2014, doi: 10.1016/j.renene.2013.11.075.

[4] David Julio CERDA SALZMANN, "Ampelmann, Development of the Access System for Offshore Wind Turbines," PhD Thesis, TU Delft, 2010.

[5] S. Mokhatab and W. A. Poe, "Chapter 14 - Process Control Fundamentals," in *Handbook of Natural Gas Transmission and Processing (Second Edition)*, S. Mokhatab and W. A. Poe, Eds. Boston: Gulf Professional Publishing, 2012, pp. 473–509. doi: 10.1016/B978-0-12-386914-2.00014-5.

[6] S. Küchler and O. Sawodny, "Nonlinear control of an active heave compensation system with time-delay," in *2010 IEEE International Conference on Control Applications*, Sep. 2010, pp. 1313–1318. doi: 10.1109/CCA.2010.5611119.

[7] M. J. Grimble, "Design of generalized minimum variance controllers for nonlinear multivariable systems," *International Journal of Control, Automation and Systems*, vol. 4, no. 3, Art. no. 3, 2006.

[8] M. J. Grimble and P. Majecki, "Nonlinear GMV control for unstable state dependent multivariable models," in *2008 47th IEEE Conference on Decision and Control*, Dec. 2008, pp. 4767–4774. doi: 10.1109/CDC.2008.4739137.

[9] "Fetch and Duration Limited Growth," *Elsevier Ocean Engineering Series*, vol. 2, pp. 83–131, Jan. 1999, doi: 10.1016/S1571-9952(99)80007-5.

[10] T. Perez, O. Smogeli, T. Fossen, and A. J. Sorensen, "An overview of the Marine Systems Simulator (MSS): A Simulink Toolbox for Marine Control Systems," *Modeling, Identification and Control*, vol. 27, no. 4, Art. no. 4, 2006.

[11] B. Šulc and J. A. Jan, "Non Linear Modelling and Control of Hydraulic Actuators," *Acta Polytech*, vol. 42, no. 3, Art. no. 3, Jan. 2002, doi: 10.14311/354.

[12] T. Sugihara, "Solvability-unconcerned inverse kinematics based on Levenberg-Marquardt method with robust damping," in *2009 9th IEEE-RAS International Conference on Humanoid Robots*, Dec. 2009, pp. 555–560. doi: 10.1109/ICHR.2009.5379515.

[13] M. J. Grimble and P. Majecki, *Nonlinear Industrial Control Systems: Optimal Polynomial Systems and State-Space Approach*. London: Springer-Verlag, 2020. doi: 10.1007/978-1-4471-7457-8.